J. Fluid Mech. (2013), *vol.* 724, R1, doi:10.1017/jfm.2013.202

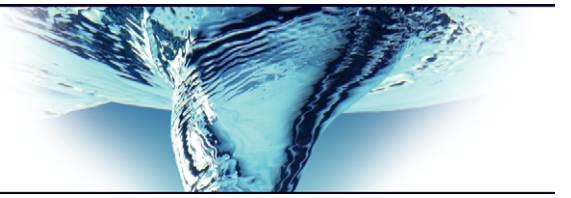

JFM RAPIDS
journals.cambridge.org/rapids

On the wetting dynamics in a Couette flow

Peng Gao† and Xi-Yun Lu

Department of Modern Mechanics, University of Science and Technology of China,
Hefei, Anhui 230026, PR China

(Received 30 January 2013; revised 13 March 2013; accepted 12 April 2013)

The dynamics of moving contact lines in a two-phase Couette flow is investigated by using a matched asymptotic procedure. The walls are assumed to be partially wetting, and the microscopic contact angle is finite but sufficiently small so that the lubrication approach can be used. Explicit formulas are derived to characterize the shear-induced interface deformation and the critical capillary number for the onset of wetting transition. It is found that the apparent contact angle vanishes for liquid–air systems and remains finite for liquid–liquid systems when the wetting transition occurs.

Key words: contact lines, interfacial flows (free surface), thin films

1. Introduction

It is well known that the dynamics of moving contact lines cannot be fully described by classical continuum hydrodynamics, since the no-slip boundary condition on the solid wall leads to an unintegrable divergence of the viscous stress at the contact line (Huh & Scriven 1971; Dussan & Davis 1974). In reality, the singularity would be ultimately released by intermolecular forces when approaching the contact line. Thus, dynamical wetting evolves in a wide range of length scales, from microscopic to macroscopic, which leads to considerable challenges in understanding the wetting dynamics.

Close to the contact line, it is primarily the balance between viscous stresses and capillary forces that determines the interface profile. The interface is highly bent by the strong viscous force so that the apparent contact angle θ_{ap}, which is usually associated with a static (or quasi-static) macroscopic interface far away from the contact line, could be significantly different from the microscopic one θ_m. The apparent contact angle can be more conveniently measured in experiments. However, the determination of θ_{ap} is non-trivial and is actually one of the most important issues in contact-line research. Apart from the flow geometry and the microscopic contact-line model, the alternation from θ_m to θ_{ap} depends primarily on the capillary

† Email address for correspondence: gaopeng@ustc.edu.cn

number $Ca = \mu U/\sigma$, a dimensionless group involving the contact-line speed U, the viscosity μ and the surface tension σ. For the wetting of a single fluid, a remarkable relation between θ_{ap} and Ca is the so-called Cox–Voinov law (Voinov 1976; Cox 1986)

$$\theta_{ap}^3 = \theta_m^3 \pm 9Ca \ln(\alpha \ell_M/\ell_m), \tag{1.1}$$

with '+' and '−' for advancing and receding contact lines, respectively. Here ℓ_M and ℓ_m are, respectively, appropriate macroscopic and microscopic length scales, and α is constant. A similar relation for two-fluid wetting was given by Cox (1986). These formulas are typically obtained by matching an inner solution in the vicinity of the contact line to an outer flow. However, α depends on the microscopic models as well as the details of macroscopic flows, and is only analytically available for very limited wetting problems, e.g. spreading drops (Hocking 1981, 1983) and capillary tubes (Voinov 1976, 2000).

A crucial wetting phenomenon that (1.1) fails to describe is the dynamic wetting transition, e.g. an increase in the speed of a receding contact line beyond a threshold, corresponding to a critical capillary number Ca_c, leading to the deposition of liquid films on the substrate (Blake & Ruschak 1979; de Gennes 1986; Sedev & Petrov 1991; Snoeijer *et al.* 2006; Snoeijer & Andreotti 2013). The reason is that (1.1) is based on the assumption of small Ca, and thus works well for low-speed wetting; a large deviation is expected at high contact-line speeds. To characterize the contact-line dynamics for wetting transition, it is necessary to obtain the inner and outer solutions at arbitrary values of Ca, which remains a challenge. For receding contact lines at small θ_m, an exact solution of the inner flow valid for arbitrary Ca is available in the framework of lubrication theory (Duffy & Wilson 1997). Based on this solution, Eggers (2004*a*, 2005) derived an analytical criterion for the wetting transition when a plate is withdrawn from a liquid bath. The theory also confirmed a classical conjecture by Derjaguin & Levi (1964) that $\theta_{ap} = 0$ at the transition. In fact, the wetting transition is associated with a saddle-node bifurcation, where a stable branch of solution meets an unstable one (Chan, Snoeijer & Eggers 2012). Snoeijer *et al.* (2007) numerically demonstrated the presence of multiple branches of solutions and bifurcations.

Two-phase Couette flows have frequently been employed to study the dynamics of moving contact lines as well as wetting transition. Although it is difficult to perform experiments, the Couette flow is convenient to implement numerically because of its simple geometry (Thompson & Robbins 1989; Jacqmin 2004; Qian, Wang & Sheng 2006; Ren & E 2007; Sbragaglia, Sugiyama & Biferale 2008). Surprisingly, as far as we know, no complete theory has been developed for such a particular wetting problem. On the one hand, Jacqmin (2004) and Sbragaglia *et al.* (2008) performed a lubrication analysis, but had to rely on a numerical approach to predict the interface profile and the criterion of wetting transition. On the other hand, comparison of numerical results with a general theory such as (1.1) exhibit ambiguities, which reside in the definition of the apparent contact angle θ_{ap}. While θ_{ap} represents theoretically the slope of the static outer interface extrapolated to the contact line (Cox 1986), two plausible versions have been used in simulations: the interfacial angle at the centre line (Thompson & Robbins 1989) and the minimum angle of the interface (Ren & E 2007). Jacqmin (2004) and Sbragaglia *et al.* (2008) also used the first definition, which is obviously arbitrary, and argued that the wetting transition occurs at $\theta_{ap} \neq 0$; the second one relies on the presence of an inflection point of the interface and could be quite different from the extrapolated one. These inconsistences are obscured by the fact that good comparisons can still be obtained by an appropriate adjustment of parameters.

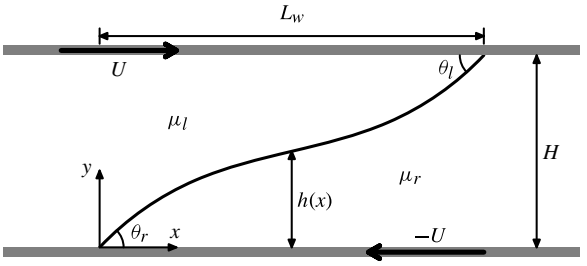

FIGURE 1. Schematic of the shear flow driven by two parallel walls moving in opposite directions with velocity $\pm U$. The line $h(x)$ represents the fluid–fluid interface.

This paper concerns the behaviour of the wetting dynamics in the Couette geometry by using a lubrication approach and a matched asymptotic procedure. The apparent contact angle is defined according to the extrapolated version. The interface deformation and the onset of wetting transition are quantified without any adjustable parameters.

2. Lubrication description of the Couette flow

We consider the two-dimensional flow in a Couette geometry, as shown in figure 1. The two walls are separated by a distance H, and move oppositely with velocities $\pm U$. The two fluids are mutually immiscible and the interface between them is described by $y = h(x)$. The contact line at the lower and upper wall lies at $x = 0$ and L_w, and the corresponding microscopic contact angles are denoted by θ_r and θ_l, respectively. Note that θ_r and θ_l are defined in different fluids. Here and below we use the subscripts l and r to denote quantities associated with the left and right fluid, respectively. To relieve the singularity at the contact lines, we employ the Navier slip boundary conditions

$$u_r + U = \lambda_s \partial u_r/\partial y \quad \text{at } y = 0, \tag{2.1}$$

$$u_l - U = -\lambda_s \partial u_l/\partial y \quad \text{at } y = H, \tag{2.2}$$

where u_l and u_r are the horizontal velocity components; λ_s is the microscopic slip length, much smaller than the macroscopic scale H.

The purpose is to seek a stationary interface profile for a given shear speed U, which thus also represents the relative velocity between the contact line and the solid wall. We assume that the viscous effect is sufficiently large for inertia to be neglected. It is further assumed that both θ_l and θ_r are small; therefore, the interface is only slightly tilted ($H \ll L_w$) so that the usual lubrication approximation can be used (Oron, Davis & Bankoff 1997). Differentiation of the interfacial normal stress condition with respect to x gives

$$\sigma \kappa'(x) = G_l(x) - G_r(x), \tag{2.3}$$

where $G_l(x)$ and $G_r(x)$ are the pressure gradient along the x-direction, σ is the surface tension and $\kappa(x) \equiv h''(x)$ is the interface curvature. Following Jacqmin (2004) and Sbragaglia *et al.* (2008), G_l and G_r as well as the velocity profiles can be determined by the remaining boundary conditions at the walls and the interface; they can be expressed explicitly in terms of h. Eventually, we obtain a single lubrication equation

for the interface height $h(x)$, which reads

$$h''' = \frac{3Ca[(n+2)nh^3 + (4\lambda n - 3)nh^2 + (8\lambda + 3)nh + 2\lambda n + 6\lambda + 1]}{h(h-1)[nh^3 + (n\lambda - n + 2\lambda + 1)h^2 - (12\lambda^2 n + 4n\lambda + 2\lambda + 1)h - 3\lambda(4\lambda + 1)]}. \tag{2.4}$$

Here h and x have been non-dimensionalized with H. The involved dimensionless parameters include the capillary number $Ca = \mu_r U/\sigma$, $n = m - 1$ with $m = \mu_l/\mu_r$ being the viscosity ratio, and the dimensionless slip length $\lambda = \lambda_s/H \ll 1$. This equation is supplemented by the boundary conditions at the contact lines,

$$h(0) = 0, \quad h'(0) = \theta_r, \tag{2.5}$$

$$h(L) = 1, \quad h'(L) = \theta_l, \tag{2.6}$$

with $L = L_w/H$ being the dimensionless contact-line position on the upper wall. Note that the third-order differential equation (2.4) is not overdetermined by the introduction of four boundary conditions, since L is not known *a priori* and should be solved as part of the solution. In addition, the singularity of the viscous force at the contact lines can be inferred from the term on the right-hand side of (2.4), which clearly diverges as $h \to 0$ or 1, especially in the absence of wall slip.

3. Liquid–air system

First we consider a liquid–air system and neglect the influence of the air ($m = 0$ or $n = -1$). In this case, the effect of the upper wall is no more than to provide a constraint on the interface slope, while its movement is insignificant since the velocity boundary condition (2.2) is unnecessary. Therefore, the upper contact line exhibits no singularity. The governing equation (2.4) reduces to

$$h''' = \frac{3Ca}{h^2 + 3\lambda h}. \tag{3.1}$$

This equation is typically encountered in studying wetting flows of a single fluid close to the moving contact line, wherein it is expected that the balance between the viscous force and capillarity dominates the dynamics (Hocking 1983; Eggers 2005; Snoeijer *et al.* 2007; Chan *et al.* 2012). For the problem considered here, (3.1) holds not only near the contact line, but also for the whole meniscus. Eggers (2004*a*, 2005) presented an asymptotic solution of (3.1) and obtained a criterion of wetting transition for a plate withdrawn from a liquid bath (see also Chan *et al.* 2012). We summarize this procedure here for completeness and extend it to the wetting problem in hand.

Introducing the similarity transformation $\xi = x\theta_r/(3\lambda)$ and $h(x) = 3\lambda h_\lambda(x\theta_r/(3\lambda))$, we have

$$h_\lambda'''(\xi) = \frac{\delta}{h_\lambda(h_\lambda + 1)}, \tag{3.2}$$

where $\delta \equiv 3Ca/\theta_r^3$ is a reduced capillary number. The boundary conditions for $h_\lambda(\xi)$ at the lower contact line are

$$h_\lambda(0) = 0, \quad h_\lambda'(0) = 1. \tag{3.3}$$

The equation can be further simplified at locations away from the contact line where $h_\lambda \gg 1$. We write $h_\lambda(\xi) = \delta^{1/3} g(\xi)$ and obtain $g'''(\xi) = g^{-2}(\xi)$, which has an exact

solution in parametric form (Duffy & Wilson 1997; Eggers 2005)

$$\left.\begin{aligned} \xi(s) &= \frac{2^{1/3}\pi \mathrm{Ai}(s)}{\beta[\alpha \mathrm{Ai}(s) + \beta \mathrm{Bi}(s)]}, \\ g(s) &= \frac{1}{[\alpha \mathrm{Ai}(s) + \beta \mathrm{Bi}(s)]^2}, \end{aligned}\right\} \quad s \in [s_1, \infty), \tag{3.4}$$

where Ai and Bi are the well-known Airy functions, α and β are constant, and s_1 is the largest root of the equation

$$\alpha \mathrm{Ai}(s_1) + \beta \mathrm{Bi}(s_1) = 0. \tag{3.5}$$

According to Eggers (2005), β is determined by matching an asymptotic form of (3.4),

$$h_\lambda'^3(\xi) = \delta g'^3(\xi) = -3\delta \ln(2^{2/3}\pi^{-1}\beta^2\xi), \tag{3.6}$$

which is valid for $1 \lesssim \xi \lesssim \beta^{-2}$, to the solution of (3.2) adjacent to the contact line, where slippage is important. The latter can be obtained via a standard procedure with expansion of (3.2) and (3.3) in δ (Hocking 1983; Eggers 2004*b*, 2005). We employ a more accurate asymptotic form of this solution for $\xi \gg 1$,

$$h_\lambda'^3(\xi) = 1 - 3\delta(1 + \ln \xi) + O(\delta^2), \tag{3.7}$$

as also obtained by Hocking (1983) for an advancing contact line. Matching (3.7) and (3.6) leads to

$$\beta^2 = 2^{-2/3}\pi \mathrm{e}^{1-(1/3\delta)} + O(\delta). \tag{3.8}$$

This value is larger by a factor of $\mathrm{e} = 2.718\,28\ldots$ than that given by Eggers (2005), who omitted the constant in the second term on the right-hand side of (3.7). This difference induces little modification of the interface deformation at small capillary numbers, but would result in an overestimation of the critical capillary number at the transition.

To fully determine the solution, we need the behaviour of the exact solution (3.4) as $\xi \to \infty$, which asymptotically reads

$$g(\xi) = \tfrac{1}{2}\kappa_\infty \xi^2 + b\xi + O(1), \tag{3.9}$$

where κ_∞ represents the interface curvature, and b is related to the interface slope close to the contact line; they have the form

$$\kappa_\infty = \left[\frac{2^{1/6}\beta}{\pi \mathrm{Ai}(s_1)}\right]^2, \quad b = -\frac{2^{2/3}\mathrm{Ai}'(s_1)}{\mathrm{Ai}(s_1)}. \tag{3.10}$$

Generally, this interface profile can be matched to an outer solution depending on the macroscopic flow geometry (Eggers 2005; Chan *et al.* 2012). For the present problem, (3.4) and hence (3.9) are valid up to the upper wall, and thus should satisfy straightforwardly the boundary conditions (2.6). Thus, at $\xi = \xi_L \equiv L\theta_r/(3\lambda)$, we have $g(\xi_L) = (\kappa_\infty \xi_L^2)/2 + b\xi_L = 1/(3\lambda\delta^{1/3})$, which yields

$$\xi_L = \frac{-b + [b^2 + 2\kappa_\infty/(3\lambda\delta^{1/3})]^{1/2}}{\kappa_\infty}. \tag{3.11}$$

Note that the $O(1)$ terms in (3.9) have been omitted for small λ. Then the contact angle condition at the upper wall gives $g'(\xi_L) = [b^2 + 2\kappa_\infty/(3\lambda\delta^{1/3})]^{1/2} = \theta_l/(\theta_r\delta^{1/3})$, or

$$\left[\frac{2^{2/3}\mathrm{Ai}'(s_1)}{\mathrm{Ai}(s_1)}\right]^2 + \frac{2^{2/3}\mathrm{e}^{1-1/3\delta}}{3\pi\lambda\delta^{1/3}\mathrm{Ai}^2(s_1)} = \frac{\theta^2}{\delta^{2/3}}, \tag{3.12}$$

with $\theta = \theta_l/\theta_r$. This serves as an equation to determine s_1 as a function of δ for given values of θ_l/θ_r and λ. Once s_1 is known, α can be obtained according to (3.5).

Typically there exist two branches of the solutions for δ less than a critical value, as illustrated in figure 2(*a*), which plots the variation of the rescaled contact-line distance $\widetilde{L} = \theta_r L$ as a function of δ. The lower branch of solutions is stable, corresponding to $\mathrm{Ai}'(s_1) < 0$ ($b > 0$); the apparent contact angle θ_{ap} can be defined as the slope of the interface approximated by (3.9) as $\xi \to 0$ (see figure 2*b*), so that $\theta_{ap}/\theta_r = \delta^{1/3}b$. The upper branch is unstable and corresponds to $\mathrm{Ai}'(s_1) > 0$ ($b < 0$). For the latter, the interface is characterized by a leading finger, and the contact line is located at an apparent position $\xi = -2b/\kappa_\infty$, where the apparent contact angle can be measured as $\theta_{ap}/\theta_r = -\delta^{1/3}b$ (Chan *et al.* 2012). Therefore, we have

$$\theta_{ap}/\theta_r = 2^{2/3}\delta^{1/3}|\mathrm{Ai}'(s_1)|/\mathrm{Ai}(s_1), \tag{3.13}$$

which is plotted in figure 2(*b*). It can be further demonstrated that the critical reduced capillary number δ_c, beyond which the stationary solution ceases to exist, occurs at $s_1 = s_{max} = -1.018\,79\ldots$ where $\mathrm{Ai}(s_1)$ attains its maximum and hence $\mathrm{Ai}'(s_{max}) = 0$. According to (3.12), δ_c is explicitly written as

$$\delta_c = 1/W_0((T\lambda\theta^2)^{-3}) \quad \text{with } T = 3\pi\mathrm{Ai}^2(s_{max})/(2^{2/3}\mathrm{e}) = 0.626\,70\ldots, \tag{3.14}$$

where $W_0(t)$ ($t \geqslant -1/\mathrm{e}$) is the principal branch of the Lambert W function defined by $W(t)\mathrm{e}^{W(t)} = t$ (Corless *et al.* 1996). Physically, for $\delta > \delta_c$, the interface is so highly bent that the interface slope at the upper wall is always larger than that prescribed by θ_l, and the interface cannot remain stationary any longer, leading to a liquid film deposited on the lower wall. Obviously, the wetting transition occurs at $\theta_{ap} = 0$, a criterion frequently postulated (Derjaguin & Levi 1964; Blake & Ruschak 1979). Note that the interface angle at the centre line of the channel, defined by Sbragaglia *et al.* (2008) as the apparent contact angle, remains finite at the transition.

Sbragaglia *et al.* (2008) calculated numerically the critical capillary number $Ca_c = \delta_c\theta_r^3/3$ using a modified lubrication approach, and compared to the theory of Eggers (2004*a*, 2005) developed for the plate withdrawal problem. However, to achieve a good comparison, they had to adjust one geometry parameter in the formula, which is not defined in the Couette system. As shown in figure 3, the present theory agrees with the numerical results very well up to $\theta_r = 45°$, even though the lubrication theory is based on the assumption of small microscopic contact angles. More importantly, there are no adjustable parameters.

4. Liquid–liquid system with matched viscosity

We now turn to the liquid–liquid system. The analysis for arbitrary values of m is tedious and can hardly provide any physical insight. For simplicity, we fix $m = 1$, while the microscopic contact angles could still be different. We note that the effect of the viscosity ratio is only quantitative, as numerically demonstrated by Sbragaglia *et al.* (2008).

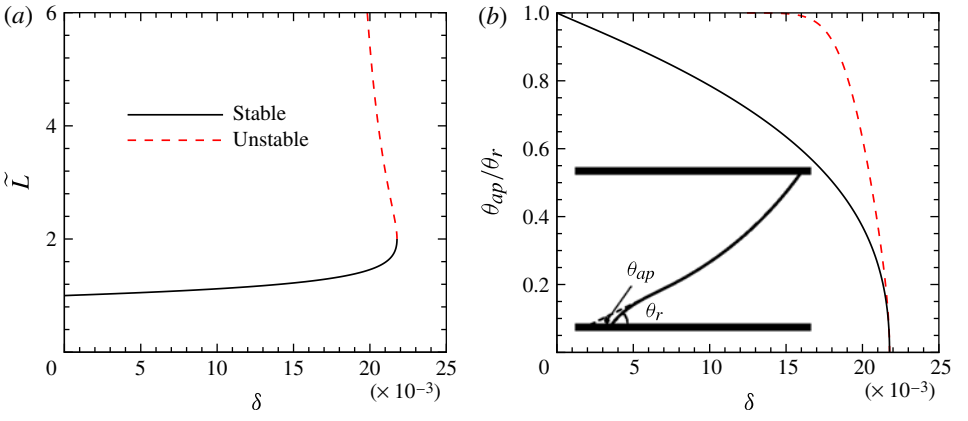

FIGURE 2. Variation of (*a*) the rescaled contact-line distance $\widetilde{L} = \theta_r L$ and (*b*) the apparent contact angle θ_{ap}/θ_r as functions of δ for $\lambda = 10^{-7}$ and $\theta = 1$. The definition of θ_{ap} is schematically shown in the inset. The stationary solutions only exist for $\delta \leqslant \delta_c = 0.0218$.

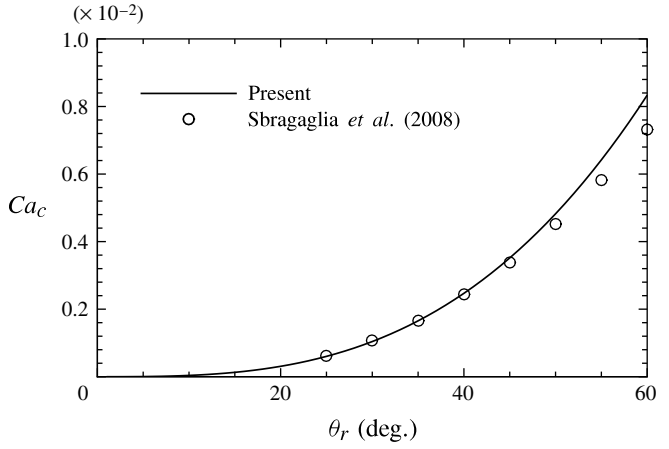

FIGURE 3. Comparison of the critical capillary number Ca_c for $\lambda = 10^{-7}$ and $\theta = 1$ with the numerical results of Sbragaglia *et al.* (2008).

The governing equation for $h(x)$ is

$$h''' = \frac{3Ca(6\lambda + 1)}{h(h-1)[(2\lambda + 1)(h-1)h - 3\lambda(4\lambda + 1)]}, \tag{4.1}$$

supplemented with boundary conditions (2.5) and (2.6). The inner solutions where slip is important and the outer solution away from the contact lines are analysed separately.

In general, the introduction of the left fluid would have a strong influence on both the inner and outer solutions (Cox 1986). However, for small microscopic contact angles, we now show that there is only one fluid coming into play close to each contact line. Take the lower contact line as an example. Using the inner variables ξ and $h_\lambda(\xi)$, (4.1) is transformed exactly into the same form of (3.2), as long as $\lambda \ll 1$. This is not surprising since the viscous force in the sharp wedge always dominates

that outside it when the contact angle is small, as in the wetting of a single liquid. Therefore, the solution (3.4) can also be used to describe the inner solution associated with the lower contact line for the liquid–liquid system. Following a similar procedure to the previous section, the inner solution near the upper contact line can be obtained.

To find the outer solution, we define $\zeta = x/L$ and $h_L(\zeta) = h(x)$ for clarity. The governing equation for the outer problem is

$$h_L''' = \frac{\widetilde{Ca}}{h_L^2\,(h_L - 1)^2}, \tag{4.2}$$

with $\widetilde{Ca} \equiv 3L^3 Ca = \widetilde{L}^3\delta$. At the two contact lines, we have $h_L(0) = 0$ and $h_L(1) = 1$. In addition, the volume of the right fluid underneath the interface is fixed: $\int_0^1 h_L(\zeta)\,\mathrm{d}\zeta = V$, where V is a normalized volume and will be determined by the matching procedure together with L. As usual, the outer solution is expanded in terms of $\widetilde{Ca}$, i.e.

$$h_L(\zeta) = h_{L0}(\zeta) + \widetilde{Ca}\,h_{L1}(\zeta) + O(\widetilde{Ca}^2), \tag{4.3}$$

assuming that $\widetilde{Ca}$ is small. As will be shown later, this assumption is invalid for the unstable solutions as well as for the stable solutions close to the wetting transition. The leading-order h_{L0} simply represents the interface profile without any flow,

$$h_{L0}(\zeta) = (1 - B)\zeta^2 + B\zeta, \tag{4.4}$$

with $B = 6V - 2$. Two apparent contact angles can be defined according to this static interface profile: $\theta_{ap}^l = h_L'(0)/L = B/L$ and $\theta_{ap}^r = h_L'(1)/L = (2 - B)/L$. As only positive apparent contact angles make physical sense, we must have $0 < B < 2$ or $1/3 < V < 2/3$.

Eggers (2005) matched directly the asymptotic form (3.9) of the inner solution as $\xi \to \infty$ to a static outer solution. This procedure cannot be used for the present problem. The inner solution associated with the lower contact line always has a positive curvature (3.10), and it can be expected that the curvature near the upper contact line is negative since the viscous bending on the interface acts in the opposite way. Thus, the outer solution must have an inflection point where the curvature changes its sign. This contradicts the fact that h_{L0} has a constant curvature. Alternatively, we need to go further to the first-order expansion h_{L1}, which typically contains a logarithmic term, and match it to the asymptotic form (3.6) of the inner solution valid for $1 \lesssim \xi \lesssim \beta^{-2}$. This new procedure is consistent if $\beta^{-2} \gg 1$ so that the outer solution and (3.6) can overlap close to the contact line, which is true for the parameters studied.

The equation for h_{L1} reads

$$h_{L1}''' = \frac{1}{h_{L0}^2\,(h_{L0} - 1)^2}, \tag{4.5}$$

whose solution can be routinely derived. Of interest is the asymptotic behaviour close to the contact lines, which takes the form

$$h_{L1}'(\zeta) \sim -[\ln(\mathrm{e}\zeta) + \Phi(B)]/B^2 \quad \text{as } \zeta \to 0^+, \tag{4.6}$$

$$h_{L1}'(\zeta) \sim -[\ln(\mathrm{e}(1 - \zeta)) + \Phi(2 - B)]/\,(2 - B)^2 \quad \text{as } \zeta \to 1^-, \tag{4.7}$$

where

$$\Phi(B) = \frac{3B-1}{(1-B)^3}\ln B - \frac{B^2(B-3)}{(1-B)^3}\ln(2-B) + \frac{B^2-B+2}{(B-2)(B-1)}. \tag{4.8}$$

For the purpose of matching, we write the inner solution associated with the lower contact line (3.6) in terms of ζ and $h_L(\zeta)$:

$$h_L'^3(\zeta) = \widetilde{L}^3[1 - 3\delta\ln(\mathrm{e}\widetilde{L}\zeta/3\lambda)], \tag{4.9}$$

recalling $\widetilde{L} = \theta_r L$. On the other hand, the asymptotic slope of the interface for the outer solution satisfies

$$h_L'^3(\zeta) = h_{L0}'^3 + 3\widetilde{Ca}h_{L0}'^2h_{L1}' + O(\widetilde{Ca}^2) = B^3 - 3\widetilde{L}^3\delta[\ln(\mathrm{e}\zeta) + \Phi(B)] + O(\delta^2), \tag{4.10}$$

as $\zeta \to 0^+$. Comparing (4.9) and (4.10), we arrive at

$$1 - B^3/\widetilde{L}^3 = 3\delta[\ln(\widetilde{L}/3\lambda) - \Phi(B)]. \tag{4.11}$$

In a similar way, the matching of the outer solution with the inner solution close to the upper contact line can be performed, leading straightforwardly to

$$\theta^3 - (2-B)^3/\widetilde{L}^3 = 3\delta[\ln(\theta\widetilde{L}/3\lambda) - \Phi(2-B)]. \tag{4.12}$$

For given values of δ, θ and λ, (4.11) and (4.12) can be regarded as a system of nonlinear equations for $\widetilde{L}$ and B, which should be solved numerically.

Specifically, if we further assume $\theta_l = \theta_r$ or $\theta = 1$, the interface would have a two-fold symmetric behaviour, which has received more attention (Thompson & Robbins 1989; Jacqmin 2004). For this symmetric case, the interface without flow is a straight line, and from (4.4) we have $B = 1$, and the two matching conditions reduce to a single equation

$$1 - 1/\widetilde{L}^3 = 3\delta\ln(\widetilde{L}/3\lambda). \tag{4.13}$$

Noting that the apparent contact angle reduces to $\theta_{ap} = 1/L$, this equation can also be written in the form of the Cox–Voinov law

$$\theta_{ap}^3 - \theta_r^3 = -9Ca\ln\frac{H\theta_r}{3\lambda_s\theta_{ap}}. \tag{4.14}$$

An important observation is the presence of θ_{ap} in the logarithmic function, which should be finite as long as the stationary interface exists. Similarly to the single-phase system, (4.13) has two branches of solutions, which are formally given as

$$\widetilde{L}_k^{-3} = -\delta W_k\left(-\frac{1}{27\lambda^3\delta\mathrm{e}^{1/\delta}}\right), \quad k = -1, 0, \tag{4.15}$$

where $W_{-1}(t)$ is the other real branch of the Lambert W function, also defined for $t \geqslant -1/\mathrm{e}$. This lower bound gives a critical capillary number

$$\delta_c = -\left[W_{-1}(-27\lambda^3/\mathrm{e})\right]^{-1}, \tag{4.16}$$

above which there are no steady solutions.

The two branches of solutions are illustrated in figure 4(*a*) for $\lambda = 10^{-6}$. The stable and unstable branches correspond to $\widetilde{L}_{-1}$ and $\widetilde{L}_0$, respectively. For comparison, (4.1) is numerically integrated via a fourth-order Runge–Kutta method. Numerical results are

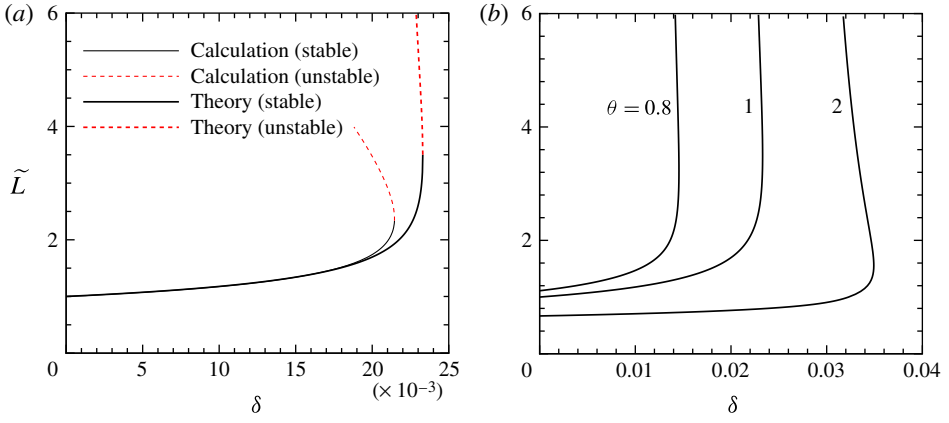

FIGURE 4. (*a*) Variation of $\widetilde{L}$ as a function of δ for the symmetric case. The theoretical solutions (thick lines) are given by (4.15). Numerical results (thin lines), obtained by directly integrating the governing equation (4.1) with $\theta_l = \theta_r = \pi/6$, are also plotted for comparison. (*b*) Effect of the contact angle ratio θ. The dimensionless slip length is $\lambda = 10^{-6}$.

obtained for $\theta_l = \theta_r = \pi/6$, which is small enough to use the lubrication approximation. As expected, the present theory shows a good prediction of the stable solution for $\delta < 0.018$. However, a pronounced deviation is observed close to the wetting transition. In particular, (4.16) overpredicts the critical capillary number by an amount of 8.6 %. This deviation is due not to the finite microscopic contact angle used in the numerical results, but to the fact that the capillary number is too large to use the expansion (4.3), which is only reasonable at small $\widetilde{Ca}$. Specifically, at $\delta = \delta_c$, we have $\widetilde{L}_c^{-3} = \delta_c$ and hence $\widetilde{Ca}_c = \widetilde{L}_c^3 \delta_c = 1$, and for the unstable branch $\widetilde{Ca} > 1$, which violate the employment of (4.3) to approximate the outer solution. With this in mind, (4.16) still provides an acceptable estimation of the critical capillary number. Moreover, differently from the single-phase case, the wetting transition occurs at finite apparent contact angles.

Finally, figure 4(*b*) depicts the influence of the contact angle ratio θ by plotting solutions for typically $\theta = 0.8$, 1 and 2. Note that the curves for $\theta \neq 1$ correspond to asymmetric interfaces. An increase of the microscopic contact angle at the upper wall delays the wetting transition, as also observed by Sbragaglia *et al.* (2008).

5. Summary

We have performed a lubrication analysis of the wetting dynamics in a Couette flow. Two special cases, i.e. the liquid–air flow and the liquid–liquid flow with matched viscosities, are considered. We use the classic definition of the apparent contact angle, which is associated with a static outer interface extrapolated to the contact line. For the liquid–air case, the wetting transition occurs at a reduced capillary number that depends only on $\lambda\theta^2$, and the associated apparent contact angle vanishes. For the liquid–liquid case, an analytical form of the contact-line position is presented and predicts the stable branch of solutions well; it shows that the apparent contact angle is finite at the wetting transition. Compared with previous numerical work, the present analysis demonstrates that the wetting transition is due to the mismatch between the inner and outer interfacial solutions.

Acknowledgements

We acknowledge support by the National Natural Science Foundation of China (No. 11102203), the Chinese Academy of Sciences (KJZD-EW-J01), the Foundation for the Author of National Excellent Doctoral Dissertation of PR China (201136), the Special Foundation of the President of the Chinese Academy of Sciences, and the Fundamental Research Funds for the Central Universities.

References

BLAKE, T. D. & RUSCHAK, K. J. 1979 Maximum speed of wetting. *Nature* **282**, 489–491.

CHAN, T. S., SNOEIJER, J. H. & EGGERS, J. 2012 Theory of the forced wetting transition. *Phys. Fluids* **24**, 072104.

CORLESS, R. M., GONNET, G. H., HARE, D. E. G., JEFFREY, D. J. & KNUTH, D. E. 1996 On the Lambert *W* function. *Adv. Comput. Math.* **5**, 329–359.

COX, R. G. 1986 The dynamics of the spreading of liquids on a solid surface. Part 1. Viscous flow. *J. Fluid Mech.* **168**, 169–194.

DERJAGUIN, B. V. & LEVI, S. M. 1964 *Film Coating Theory*. Focal.

DUFFY, B. R. & WILSON, S. K. 1997 A third-order differential equation arising in thin-film flows and relevant to Tanner's law. *Appl. Math. Lett.* **10**, 63–68.

DUSSAN, E. B. & DAVIS, S. H. 1974 Motion of a fluid–fluid interface along a solid surface. *J. Fluid Mech.* **65**, 71–95.

EGGERS, J. 2004*a* Hydrodynamic theory of forced dewetting. *Phys. Rev. Lett.* **93**, 094502.

EGGERS, J. 2004*b* Toward a description of contact line motion at higher capillary numbers. *Phys. Fluids* **16**, 3491–3494.

EGGERS, J. 2005 Existence of receding and advancing contact lines. *Phys. Fluids* **17**, 082106.

DE GENNES, P. G. 1986 Deposition of Langmuir–Blodgett layers. *Colloid Polym. Sci.* **264**, 463–465.

HOCKING, L. M. 1981 Sliding and spreading of thin two-dimensional drops. *Q. J. Mech. Appl. Maths* **34**, 37–55.

HOCKING, L. M. 1983 The spreading of a thin drop by gravity and capillarity. *Q. J. Mech. Appl. Maths* **36**, 55–69.

HUH, C. & SCRIVEN, L. E. 1971 Hydrodynamic model of steady movement of a solid/liquid/fluid contact line. *J. Colloid Interface Sci.* **35**, 85–101.

JACQMIN, D. 2004 Onset of wetting failure in liquid–liquid systems. *J. Fluid Mech.* **517**, 209–228.

ORON, A., DAVIS, S. H. & BANKOFF, G. 1997 Long-scale evolution of thin liquid films. *Rev. Mod. Phys.* **69**, 931–980.

QIAN, T., WANG, X.-P. & SHENG, P. 2006 A variational approach to moving contact line hydrodynamics. *J. Fluid Mech.* **564**, 333–360.

REN, W. & E, W. 2007 Boundary conditions for the moving contact line problem. *Phys. Fluids* **19**, 022101.

SBRAGAGLIA, M., SUGIYAMA, K. & BIFERALE, L. 2008 Wetting failure and contact line dynamics in a Couette flow. *J. Fluid Mech.* **614**, 471–493.

SEDEV, R. V. & PETROV, J. G. 1991 The critical condition for transition from steady wetting to film entrainment. *Colloids Surf.* **53**, 147–156.

SNOEIJER, J. H. & ANDREOTTI, B. 2013 Moving contact lines: scales, regimes, and dynamical transitions. *Annu. Rev. Fluid Mech.* **45**, 269–292.

SNOEIJER, J. H., ANDREOTTI, B., DELON, G. & FERMIGIER, M. 2007 Relaxation of a dewetting contact line. Part 1. A full-scale hydrodynamic calculation. *J. Fluid Mech.* **579**, 63–83.

SNOEIJER, J. H., DELON, G., FERMIGIER, M. & ANDREOTTI, B. 2006 Avoided critical behavior in dynamically forced wetting. *Phys. Rev. Lett.* **96**, 174504.

THOMPSON, P. A. & ROBBINS, M. O. 1989 Simulations of contact-line motion: slip and the dynamic contact angle. *Phys. Rev. Lett.* **63**, 766–769.

VOINOV, O. V. 1976 Hydrodynamics of wetting. *Fluid Dyn.* **11**, 714–721.

VOINOV, O. V. 2000 Wetting: inverse dynamic problem and equations for microscopic parameters. *J. Colloid Interface Sci.* **226**, 5–15.